Analytical Methods

ROYAL SOCIETY OF CHEMISTRY

PAPER

View Article Online
View Journal | View Issue

Cite this: *Anal. Methods*, 2020, **12**, 2152

Versatile additively manufactured (3D printed) wall-jet flow cell for high performance liquid chromatography-amperometric analysis: application to the detection and quantification of new psychoactive substances (NBOMes)†

Hadil M. Elbardisy,[ab] Eduardo M. Richter,[*ac] Robert D. Crapnell,[a] Michael P. Down,[a] Peter G. Gough,[a] Tarek S. Belal,[d] Wael Talaat,[b] Hoda G. Daabees[e] and Craig E. Banks[*a]

Additive manufacturing (AM/3D printing) is an emerging technology of vast applicability, receiving significant interest in a plethora of industrial domains and scientific research since it allows the rapid translation of designs produced *via* computer software, into AM/3D printed objects. To date, AM/3D printed devices have been examined for their utilisation as convenient and cost-effective tools towards the detection and quantification of prevalent drugs of abuse. Herein, a novel AM/3D printed wall-jet flow cell was fabricated specifically for employment in high performance liquid chromatography-amperometric detection (HPLC-AD) of various analytes (New Psychoactive Substances). Five sensing platforms were investigated, utilising different working electrodes, namely; screen-printed graphite electrodes (SPEs), AM/3D Proto-Pasta, AM/3D Black Magic, graphite sheet and AM/3D printed nanographite (NG)/polylactic acid (PLA) towards the detection of New Psychoactive Substances. The flow cell was also optimised with respect to the cell geometry demonstrating significant benefits such as simple production and operation and the ability to tailor the platform to a variety of working electrodes. The AM/3D printed sensing platforms were characterised towards the (electro) analytical detection of four *N*-benzylmethoxy-derivatives: 25F–NBOMe, 25C–NBOMe, 25B–NBOMe and 25I–NBOMe. Furthermore, the (electro) analytical performance of the flow cell was compared with the findings in our previous work comprising of a commercially available impinging jet flow cell. The SPEs and the graphite sheet were found to demonstrate superior electrochemical (analytical) sensitivity and higher reproducibility towards the quantification of the drugs in question, followed by the NG/PLA AM, Proto-Pasta and the Black Magic. The working electrodes that exhibited satisfactory (electro) analytical responses were employed for the analysis of NBOMe derivatives in three simulated blotter papers.

Received 9th March 2020
Accepted 26th March 2020

DOI: 10.1039/d0ay00500b

rsc.li/methods

Introduction

Additive manufacturing (AM, 3D printing) is a rapidly growing technology that has had a major impact on manufacturing in the last few decades. It has evolved at an unprecedented rate, due to the freedom it offers in designing, rapid prototyping, mass customization, minimizing material waste and improving cost effectiveness.[1] AM/3D printing builds three dimensional objects through digitally controlled deposition of materials in a layer-by-layer fashion until the final structure is created.[2,3] To date, the most utilised AM/3D printing technique is fused deposition modelling (FDM). The simplicity and high speed of operation, as well as the availability of affordable 3D printers, has allowed FDM to become the most commonly used AM/3D printing technology.[3] AM/3D printing can produce complex structures using a diverse range of materials (*e.g.*,

[a]*Faculty of Science and Engineering, Manchester Metropolitan University, Chester Street, Manchester, M1 5GD, UK. E-mail: c.banks@mmu.ac.uk; Web: www.craigbanksresearch.com; Tel: +44(0) 1612471196*

[b]*Pharmaceutical Analysis Department, Faculty of Pharmacy, Damanhour University, Damanhour, 22511, Egypt*

[c]*Institute of Chemistry, Federal University of Uberlandia, Av. João Naves de Avila, 2121, 38400-902, Uberlandia, MG, Brazil. E-mail: emrichter@ufu.br*

[d]*Department of Pharmaceutical Analytical Chemistry, Faculty of Pharmacy, Alexandria University, Alexandria, 21521, Egypt*

[e]*Pharmaceutical Chemistry Department, Faculty of Pharmacy, Damanhour University, Damanhour, 22511, Egypt*

† Electronic supplementary information (ESI) available. See DOI: 10.1039/d0ay00500b

thermoplastics, metals, ceramics, living cells, *etc.*). This has enabled it to be utilized in a wide variety of fields, including aerospace,[4] medicine,[5] chemical engineering[6] and environmental sciences.[7] As this technology is continually advancing, it has opened new horizons in other research domains, such as analytical chemistry[8,9] and electrochemistry.[10,11] Examples of AM/3D printed electrochemical sensors and devices found in literature include; sensing electrodes,[10] electrochemical cells,[2] microfluidic devices,[12] microneedles,[13] supercapacitors[14] and reaction ware for chemical synthesis and analysis.[15]

The fabrication of flow cells for analytical purposes has been presented by commercial companies, such as Metrohm,[16]Antec Scientific,[17] BASI®[18] and ERC Co.[19] There have also been reports in the scientific literature of fabricating flow cells for further applications in flow-injection analysis,[20,21] electrochemiluminescent analysis,[22] studying biological redox reactions,[23] mechanistic and kinetic studies,[24] electrochemical degradation of dye[25] and environmental sciences.[26] Interestingly, liquid chromatography with amperometric detection (LC-AD) has been one of the analytical approaches that has employed the use of flow cells; owing to its high sample throughput, affordable detector price and wide range of electroactive analytes that can be detected. Joynes *et al.* first reported a simple cell design incorporating a silicone-carbon membrane electrode for the quantitation of some organic and inorganic compounds.[27] Thereafter, optimization of the geometrical configurations was reported, such as the classical thin-layer[28] and the wall-jet flow cells.[29] Further modification to these classical prototypes took place; such as wall-jet flow cells based on rotating disk electrodes.[30,31] ESI Table S1† summarizes research articles described in literature dealing with flow cells manufactured for HPLC-AD. This includes the flow cells geometries and manufacturing materials, the utilised working electrodes, the analytes detected, and the pros and cons in the flow cells design.

Currently, there are several AM/3D printed electrochemical flow cells reported in the literature; for instance, chemiluminescence detection flow cells[32] and flow cells for synthesis.[33] To date, a fully AM/3D printed fabricated flow cell for LC-AD has not yet been reported. To this end, we report a novel multi-use wall-jet AM/3D printed flow cell that was constructed specifically for LC-AD. This flow cell is versatile and can incorporate electrodes of different materials. In this work, the tested working electrode substrates were screen-printed graphite macroelectrodes (SPEs), graphite sheets, and FDM AM/3D printable materials; including Proto-Pasta and Black Magic commercial conductive filaments and a homemade conductive filament synthesised from nanographite (NG) and polylactic acid (PLA) (NG/PLA). The proposed flow cell model and the sensitivity of the sensing platforms were evaluated by analyzing a mixture of four 2,5-dimethoxy-*N*-(2-methoxybenzyl) phenethylamine derivatives (NBOMe derivatives; 25F–NBOMe, 25C–NBOMe, 25B–NBOMe and 25F–NBOMe) as model analytes. NBOMEs are a new class of novel psychoactive substances, they are potent agonist of the 5-HT2A receptor and even doses in micrograms can produce psychoactive effects.[34] These compounds display significant toxicological consequences as several deaths have been reported upon their intake.[35,36] Accordingly, employing those NBOMes in this study can be beneficial for deduction of the analytical methodology of highest sensitivity for their quantification. Moreover, the analytical performance of the constructed AM/3D printed LC-AD flow cell was compared to the results obtained previously in our published report using a commercially available impinging jet flow cell for the electrochemical (amperometric) determination of NBOMe derivatives.[37] Lastly, the working electrodes that demonstrated satisfactory electrochemical performance and sensitivity were utilised for the quantification of the four NBOMe derivatives in simulated blotters.

Experimental

Chemicals and materials

All chemicals were purchased at analytical grade from Sigma-Aldrich (UK) or Fluorochem Limited (UK) and used as received without any further purification. The investigated NBOMe derivatives (Scheme 1): 25F–NBOMe·HCl (2-(4-fluoro-2,5-dimethoxyphenyl)-*N*-[(2-methoxyphenyl)methyl]ethanamine hydrochloride), 25C–NBOMe·HCl (2-(4-chloro-2,5-dimethoxyphenyl)-*N*-[(2-methoxyphenyl)methyl]ethanamine hydrochloride), 25B–NBOMe·HCl (2-(4-bromo-2,5-dimethoxyphenyl)-*N*-[(2-methoxyphenyl) methyl]ethanamine hydrochloride) and 25I–NBOMe·HCl (2-(4-iodo-2,5-dimethoxyphenyl)-*N*-[(2-methoxyphenyl)methyl] ethanamine hydrochloride) were synthesised, at Manchester Metropolitan University in accordance with Elbardisy *et al.*[37] Lysergic acid diethylamide (LSD) (Scheme 1) was obtained from LGC GmbH (Germany) and was used as received without any further purification. All aqueous solutions were prepared with deionised water of resistivity $\geq 18.2\ \Omega$ cm. All solutions (unless stated otherwise) were vigorously degassed, for 10 minutes, with highly pure nitrogen to remove oxygen prior to analysis.

Instrumentation

High performance liquid chromatography-amperometric detection (HPLC-AD). Reverse phase HPLC was performed with an Agilent HP Series 1100 Liquid Chromatography Instrument (Agilent Technologies, UK). The Agilent 1100 Series Diode Array Detector G1315A was monitored at 205 nm. The stationary phase used was ACE C18-AR column (150 × 4.6 mm,

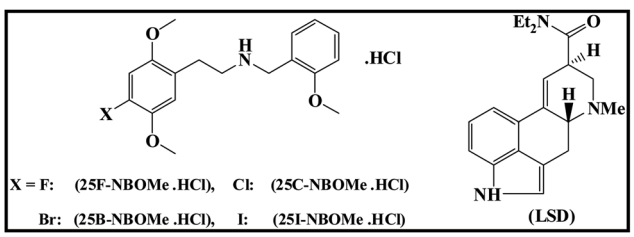

Scheme 1 Chemical structures of 2,5-dimethoxy-*N*-(2-methoxybenzyl)phenethylamine (NBOMe) derivatives: 25F–NBOMe·HCl, 25C–NBOMe·HCl, 25B–NBOMe·HCl, 25I–NBOMe·HCl and lysergic acid diethylamide (LSD). The synthesis and characterisation of these compounds is reported in Elbardisy *et al.*[37]

particle size: 5 μm, HICHROM Ltd., UK) controlled at 60 °C. The mobile phase was [ammonium formate (5 mM) and potassium chloride (100 mM) (pH 7.0): acetonitrile; 30 : 70% v/v] flowing at a rate of 2.5 mL min^{-1} (total run time: 12 min) with an injection volume of 10.0 μL. The HPLC was coupled to a home-made wall-jet AM/3D printed flow-cell housing the electrode to give the HPLC-AD system. The connection between the two parts was achieved *via* PTFE tubing (0.3 mm). Amperometric measurements were carried out using a Palmsens Emstat 3 (Palmsens BV, Netherlands) and controlled by PSTrace (version 4.4) software. All the amperometric measurements were carried out using the following parameters: potential (E, +1.0 V); equilibration time ($t_{equilibration}$, 10.0 s); data interval ($t_{interval}$, 0.08 s); current range (100 nA to 1 mA) and total run time (t_{run}, 5000 s).

An 'μAutolab type III' (MetrohmAutolab, Netherlands) potentiostat/galvanostat interfaced to a PC loaded with NOVA 2.1 software was used to conduct chronoamperometry and cyclic voltammetric measurements for activation the AM/3D printed electrodes (Proto-Pasta and Black Magic). The measurements were performed using a 10 mL voltammetric cell and a conventional three electrode set-up.

Design and fabrication of multiuse AM/3D printed flow cell for HPLC-AD. The design of the AM/3D flow cell was drawn using Tinkercad™ online software.[38] AM/3D printing was performed using a commercially available high-resolution Form 2 SLA 3D printer (Formlabs, USA). The printing material was photopolymer resin (Clear FLGPCL02) (Formlabs, USA). Following printing, the AM/3D printed flow cell was washed with isopropanol for 30 minutes, followed by tap water and then the support material that fills up the void spaces in the device design was removed.

The AM/3D printed flow cell, with an internal volume of 1.2 mL, was composed of the following parts (see Fig. 1A). The top cover was comprised of three openings; two openings at the extremities for the counter and reference electrodes (these openings are left unoccupied in the case of using SPEs). The middle inlet was for the passage of the HPLC outlet PTFE tubing; this opening was extended downwards with a cylindrical support to hold the PTFE tubing close to the surface of the working electrode. The distance between the HPLC outlet PTFE tubing and the electrode surface was kept fixed at 1.5 mm. Access to the main body of the flow cell (height: 21.3 mm, internal diameter: 14 mm, external diameter: 17 mm) was provided by an orifice (fitted by a rubber O-ring) at the bottom for exposing the working electrode surface (shown in Fig. 1B and C). The electrode was situated at the bottom of the flow cell and exposed through the orifice, fitted with a rubber O-ring to prevent leakage. This orifice could have different internal diameters; 8.0 mm for the SPEs and 5.0 mm for the rest of the working electrodes. The flow cell had a cylindrical outlet (length: 16 mm) tilted at an angle of 5° that allowed the efflux of the mobile phase to pass easily out of the flow cell and decrease the internal pressure. It was connected to a waste container *via* rubber tubing. The outlet was helped by a support underneath to strengthen the outlet; making it more rigid and decreasing the possibility of its breakage. The bottom cover of the flow cell had a thin rectangular cavity, in which the working electrode was inserted, that accommodated a steel rectangular plate (11 × 34 mm^2) for electrical contact of the working electrodes by their reverse side. This bottom cover had 3 holes for the insertion of the 3 screws to secure it tightly with the body of the flow cell. Fig. 1D represents a schematic cross-sectional diagram for the proposed AM/3D printed flow cell.

It should be noted that the reference and counter electrodes were utilised with all working substrates except the SPEs, which has the three electrode constituents (graphite working electrode, a graphite counter electrode and a Ag/AgCl reference electrode). The SPEs were connected to the potentiostat by the means of an edge connector, whilst connection to the rest of the working electrodes to the potentiostat was achieved by the means of crocodile clips in addition to the reference and counter electrodes.[39] The electrical contact between the solution and the SPE surface was defined by the internal diameter of the bigger O-ring (8.0 mm). Likewise, the other working materials surfaces were limited by the smaller O-ring internal diameter (5.0 mm). However, the counter and reference electrodes had more contact with the solution as the mobile phase fills the half of the flow cell.

Fabrication of the electrochemical sensing platforms. Five working electrodes were used to assess the validity and versatility of the proposed AM/3D printed flow cell design. The performance of those platforms was compared in terms of reliability, reproducibility and detection limits. The electrodes utilised were screen-printed graphite macroelectrodes (SPEs), graphite sheets, and three AM/3D printed electrodes. Two of the AM/3D printed electrodes were produced from the commercial filaments Proto-Pasta (ProtoPlant, USA) and Black Magic (Graphene Laboratories Inc, USA) and the third one was a filament composed of nanographite (NG) and polylactic acid (PLA) (NG/PLA AM/3D printed electrode).[40]

The SPEs utilised were fabricated in-house, as previously reported,[41] and consisted of a 3.1 mm diameter graphite working electrode, a graphite counter electrode and a Ag/AgCl reference electrode. The SPE was cut wider than its width as shown in Fig. S1† in order to fill the rectangular cavity and decrease the chance of cell leakages; the dimension of the grey partition was measured at 34 × 11 mm^2. It should be noted that a new SPE was used for each experiment performed. The commercial graphite sheet (18 × 11.5 cm^2) was purchased from Panasonic Mouser Electronics (Mansfield, Texas). It was used as received from the company without any pre-treatments and cut to size, 34 × 11 mm^2.

The commercial conductive filaments, Proto-Pasta (carbon black/PLA, filament diameter: 1.75 mm, print temperature 190–230 °C) and Black Magic (graphene/PLA, filament diameter: 1.75 mm, print temperature: 220 °C) were FDM 3D printed into a square using a conventional FDM ZMorphVX 3D printer (Z-Morph Industries, Poland). The 3D printed Proto-Pasta electrode was electrochemically activated as previously reported in the literature,[42] by applying the potentials +1.4 V/200 s and −1.0 V/200 s in 0.5 mol L^{-1} NaOH using two 3D printed Proto-Pasta electrodes as the reference and counter electrodes. Similarly, the 3D printed Black Magic electrode was pre-treated following

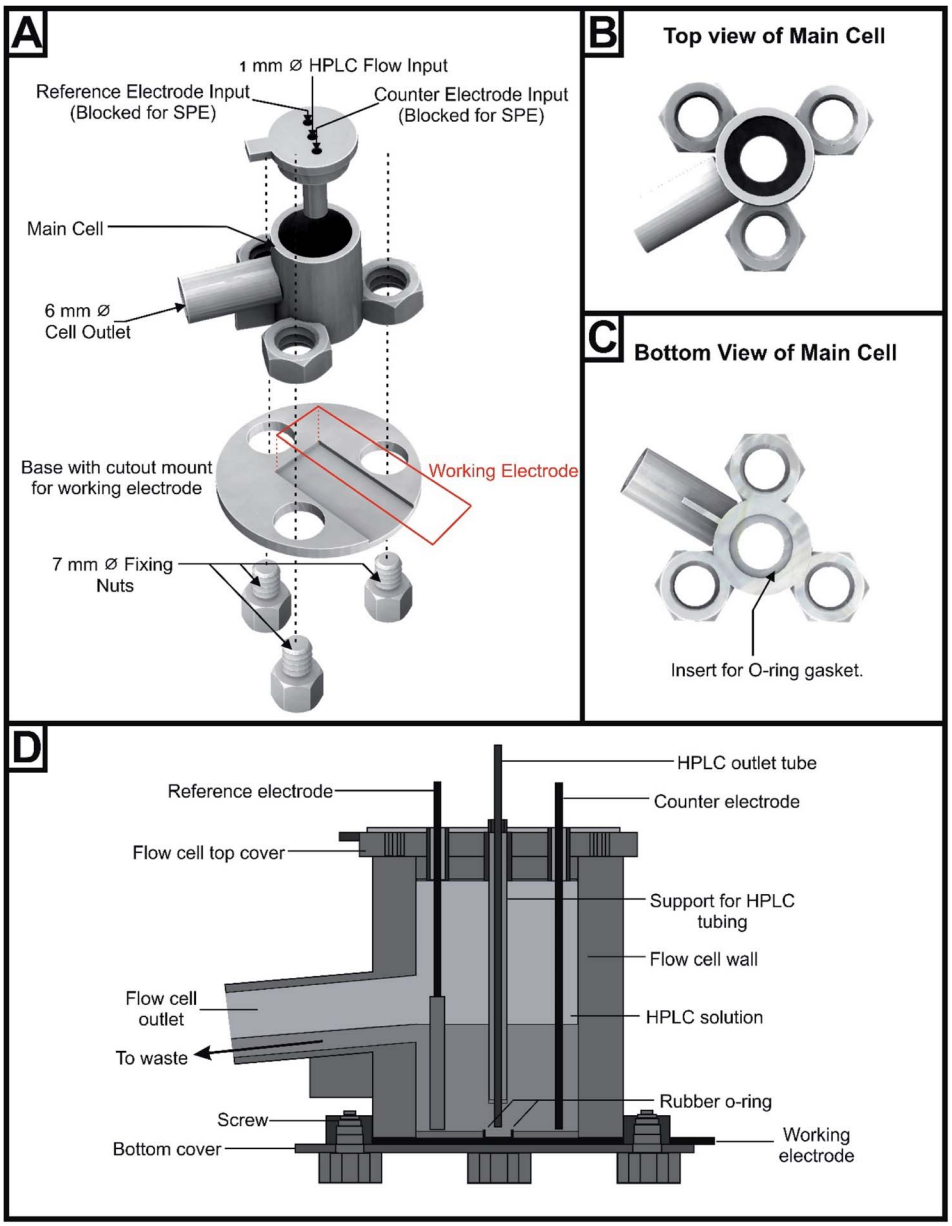

Fig. 1 (A) Schematic diagram of the proposed AM/3D printed LC/AD wall-jet flow cell displaying all its parts. (B) Upper view for the AM/3D printed flow cell showing the lower orifice. (C) Bottom view for the AM/3D printed flow cell demonstrating the lower orifice and the rubber O-ring insertion gasket. (D) Cross-sectional diagram of the proposed AM/3D printed LC-AD wall-jet flow cell.

the methodology created by dos Santos *et al.*[10] This was achieved by oxidation of the electrode at +1.8 V for 900 s and reduction from 0.0 V to −1.8 V at 50 mV s^{-1} *vs.* saturated calomel electrode (SCE) in 0.1 mol L^{-1} PBS (pH 7.4).

NG/PLA AM-electrode was prepared using the following procedure. Nanographite (NG)/PLA filaments were fabricated by mixing NG and PLA, utilising a facile solution based mixing step. Briefly, the 3.75 g of mesoporous NG were dispersed within excess xylene (this mixture was sonicated for 10 minutes to ensure complete dispersion of the carbon in xylene) and heated under reflux at 150 °C for 3 hours. Following this, 11.25 g of PLA was added to the mixture and left for a further 3 hours. The resulting homogenous mixture was then precipitated in methanol, filtered under vacuum and left to dry overnight to ensure that any remaining solvent had evaporated. The resulting NG/PLA powder was then extruded with a Mini CTW twin-screw extruder (ThermoScientific) at a temperature of 200 °C and a screw speed of 30 rpm. The diameter of the filament (1.75 mm) was controlled with a specific die with a set diameter. The resulting filament was FDM 3D printed using the ZMorph VX® 3D printer with a direct drive extruder at a temperature of 190 °C.

The three AM/3D printed working electrodes were cut to the dimensions 34 × 11 × 1 mm^3 and then their surfaces were entirely smoothed using wet sand paper. In order to achieve the three-electrode set-up for amperometric detection, all the used

sensing platforms, except for the SPE, worked in conjunction with nickel wire which served as auxiliary/counter electrode and Proto-Pasta filament dipped into silver ink and left to dry overnight as the reference electrode.

Preparation of the mobile phase [acetonitrile: 5 mM ammonium formate–100 mM potassium chloride buffer (pH 7.0), 30 : 70% v/v]. The buffer system (5 mM ammonium formate and 100 mM potassium chloride) was prepared and the pH was adjusted to pH 7.0 (±0.02) by dropwise addition of 0.2 M NaOH. Afterwards, appropriate proportions of the aqueous phase and the organic modifier were mixed to obtain a mobile phase of the desired ratio. Before running the HPLC, the mobile phase was vacuum filtered through a 0.45 mm pore filter paper.

Preparation of standard stock solution and calibration curve working solutions of NBOMEs for HPLC-AD. 10.0 mg of each NBOMe derivative were weighed accurately into one 20.0 mL clear glass volumetric flask and diluted to volume with mobile phase to give a stock solution containing 0.5 mg mL^{-1} of each drug. Working solutions for calibration standards were prepared by further dilution of the stock solution with the mobile phase to give solutions containing 10, 20, 50, 100, 150, 200 and 300 μg mL^{-1} of each analyte. Working solutions were injected directly into the HPLC and the current densities j (μA mm^{-2}) of the studied drugs were plotted against their corresponding concentrations to construct the calibration curves.

Forensic application

Application to simulated blotter papers. Blotter papers were cut into pieces with dimensions 1 cm × 1 cm, then were soaked in 3 different vials (each with 3 replicates). Each vial contained 2.0 mL of the following solutions. Vial one contained 200 μg mL^{-1} LSD and 600 μg mL^{-1} 25I–NBOMe, the second vial contained 100 μg mL^{-1} LSD, 500 μg mL^{-1} 25I–NBOMe and 600 μg mL^{-1} 25F–NBOMe and the third vial contained 500 μg mL^{-1} 25B–NBOMe. The blotter papers were kept submerged in the solutions overnight. The following day, the contents in the blotter papers were extracted by transferring each blotter paper to an Eppendorf containing 1.0 mL methanol and sonicated in ultrasonic bath for 20 minutes. Finally, the obtained solutions were diluted to half with the mobile phase to get concentrations of the drugs within the linearity ranges and injected into the HPLC-AD system.

Results and discussion

The overlay of cyclic voltammograms for a solution containing 100 μg mL^{-1} of each NBOMe derivative in 0.04 M Britton–Robinson buffer (pH 7.0) (depicted in Fig. S2†) illustrated that these compounds have two distinct oxidation peaks; peak I (E_1 ≈ +0.815 V) and peak II (E_2 ≈ +1.017 V), using screen printed graphite electrodes (SPEs) *vs.* Ag/AgCl reference electrode (scan rate: 50 mV s^{-1}). The electrochemical oxidation mechanism of NBOMes was explained in detail by Andrade *et al.*[43] Briefly, the first observed oxidation peak (peak I) develops as a result of the oxidation of the secondary amine into a primary amine. Whilst, the second oxidation peak (peak II) occurs due to the replacement of the halogen atom in the NBOMe compounds by a hydroxyl group, which afterwards produces a ketone.

In our previous work,[37] an HPLC-AD method employing a commercial impinging jet flow cell (3.3 × 6.0 × 3.3 cm, flow chamber volume = 8 μL, Metrohm UK, Runcorn, UK) was developed and applied for separation and quantification of the four phenethylamine derivatives (NBOMes), owing to the failure of the conventional voltammetric methods to separate them. In this study, we adopted the same HPLC-AD methodology for separation of the four drugs using our homemade AM/3D printed wall-jet flow cell and its performance characteristics were contrasted with those obtained from the commercial flow cell.[37]

AM/3D printed flow cell design optimization

Amperometric detection has been the most commonly investigated electrochemical detection technique in conjunction with liquid chromatography. It has been shown that the material of the working electrode and the geometry of the flow cell play a crucial role in the sensitivity and selectivity of the amperometric measurements.[44] Two flow cell designs, the classical thin-layer and wall-jet, have dominated the literature in this area. The thin-layer cell geometry was characterised by the HPLC eluent flowing parallel to the active surface of the working electrode. However, in the wall-jet configuration the eluent flowstream jets/impinges the surface of the working electrode perpendicularly, then it flows radially.[44] The latter configuration has been proven to enhance the mass transport to the electrode surface, consequently improving the sensitivity.[45,46] In addition, jetting of the solution on to the electrode surface minimised the electrode fouling and overcame memory effect by continuous cleaning of the working electrode surface.[44,47] Because of these advantages, in this work an AM/3D printed wall-jet based flow cell was designed for use in conjunction with liquid chromatography. The key parameters involved in the design were the incorporation of different working electrode substrates, the sealing of the system and the distance between the solution inlet and working electrode surface. To achieve this, the working volume of the cell had to be increased to incorporate an external reference and counter electrode. This was due to the commercial flow cells being produced to only perform with the commercial SPEs that contained a working, reference and counter electrode.

Firstly, the flow cell geometry was designed in a way to decrease the systems internal pressure. This was achieved by increasing the cylindrical outlet drainage diameter (6 mm) and tilting it at an angle of 5° from the horizontal. This enhanced the removal of the solution from the cell. The outlet was positioned 5 mm from the lower cell surface, which allowed only half of the cell capacity to be filled during the chromatographic run. This decreased the upward forces and pressure on the lower cell orifice, reducing the chance of leakages. A rubber O-ring was also used in the lower cell orifice to prevent leakages when the cell body was held together.

Secondly, the resolution of the printer, the AM/3D printing technique and the printing material were important during the development of the flow cell. To prevent leakages from the cell, a smooth uniform surface of the lower orifice was indispensable. A form 2 3D printer was operated by the SLA AM/3D printing technique alongside the photopolymer resin (Clear FLGPCL02) printing material. This offered AM/3D printed products of excellent quality and very smooth surfaces. The rough surfaces of the AM/3D printed electrodes utilised in this study, printed utilizing FDM technology (using commercially available and bespoke made filaments; Proto-Pasta, Black Magic and homemade NG/PLA AM-electrode) were thoroughly polished with wet sand paper before analytical measurements.

A critical factor of valuable consideration that was studied in most designed wall-jet flow cells is the distance between the HPLC outlet tubing and the electrode surface.[48,49] The HPLC outlet PTFE tubing was fixed at variable distances above the electrode surface (0, 1, 2 and 3 mm) and the amperometric signal (current density j (μA mm^{-2})) of 500 μg mL^{-1} paracetamol was monitored utilising the flow cell with medium orifice. As seen in Fig. 2, the current density, j, was nearly unchanged over the range of the distances examined, emphasizing the robustness of the developed flow cell. Accordingly, the distance between the HPLC tubing outlet and the electrode surface was fixed at 1.5 mm throughout this study. Importantly, the durability and strength of the material of the flow cell was tested owing to the presence of organic solvent in the mobile phase that might cause weakness in the walls ending up with leakages. This was tested by leaving the assembled flow cell in contact with the mobile phase used in this study for three consecutive days and observing any changes occurs within the flow cell walls. No leaching of material or cracks within the body of the flow cell were noticed during this period.

The flow cell developed in this study had the advantage of being versatile, as its configuration permits the ease and rapid replacement of the three electrodes. This would allow the user to change to their preferred electrode without fabricating a new cell. Moreover, this simple design can be reproducibly fabricated. Also the flow cell is inexpensive to produce, has reduced manufacturing time, can tolerate high flow rates of the mobile phase without leakages (2.5 mL min^{-1}) and can be tailored with different sizes to accommodate variety of electrodes.

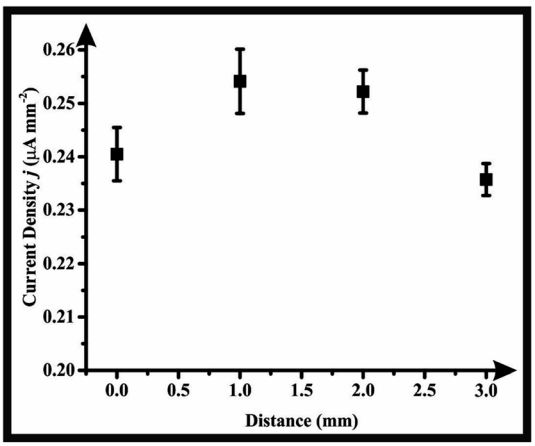

Fig. 2 Studying the effect of the distance (mm) between the HPLC outlet PTEF tubing and the electrode surface on the amperometric response current density j (μA mm^{-2}).

Electroanalytical performance and validation parameters of the working electrodes used in this study

The HPLC-AD amperograms of a solution containing 300 μg mL^{-1} of the four NBOMe derivatives (*i.e.* 25F–NBOMe, 25C–NBOMe, 25B–NBOMe and 25I–NBOME) are depicted in Fig. 3. These were obtained utilising the developed AM/3D printed LC-AD wall-jet flow cell system in conjunction with the following working electrode substrates: SPEs (Fig. 3A), Proto-Pasta (CB/PLA) before activation (Fig. 3B), Proto-Pasta (CB/PLA) after activation (Fig. 3C), Black Magic (graphene/PLA) before pre-treatment (Fig. 3D), Black Magic (graphene/PLA) after pre-treatment (Fig. 3E), the graphite sheet (Fig. 3F) and NG/PLA AM-electrode (Fig. 3G). These working electrodes were chosen to exhibit the versatility of the AM/3D Printed flow cell, in addition to presenting the opportunity to realise a fully AM/3D printed sensor platform. The retention time of the eluted NBOMe derivatives in the depicted amperograms were as follows: 25F–NBOMe (t_R = 3.84 min), 25C–NBOMe (t_R = 5.97 min), 25B–NBOMe (t_R = 7.02 min) and 25I–NBOMe (t_R = 9.46 min) which were well corroborated with our previous work achieved using the commercial impinging jet flow cell.[37]

The calibration curves for all the tested working substrates were constructed by plotting the current density j (μA mm^{-2}) *vs.* the corresponding concentrations of each analyte (see Fig. S3A–G†). The validation parameters such as the intercepts (a), slopes (b), co-efficient of regression (r^2) and limits of detection (LODs) for the analytical determination of the four NBOMe derivatives obtained for the different working electrodes using the proposed AM/3D printed flow cell HPLC-AD system are summarised in Table 1A–D. The LOD was calculated as per the following equation; LOD = 3.3Sa/b, where (Sa) is the standard deviation of the intercept and (b) is the slope of the regression line of the calibration curves of NBOMe derivatives. Repeatability tests (intra-day precision) were done by analyzing three different concentration levels of each derivative, three times (n = 3) on the same day, within the same laboratory, using the same instruments by the same analyst and the relative standard deviation percentages (RSD%) were calculated (Table S2†).

Screen-printed graphite macroelectrodes (SPEs). Upon HPLC-AD analysis of NBOMe derivatives with SPEs utilising the proposed AM/3D printed flow cell, it was noticed that the amperogram had a low background current (Fig. 3A). The sensitivity (the slope of the calibration curve of each NBOMe derivative) of SPEs working platform was the best among all tested electrodes; it was better than that obtained using the Proto-Pasta and Black Magic AM/3D printed electrodes, even after their chemical pre-treatments (Table 1B), also it was higher than those of the graphite sheet (with exception to 25F–NBOMe) and the NG/PLA AM-electrode. In order to compare the analytical performance of SPEs employing our designed AM/3D

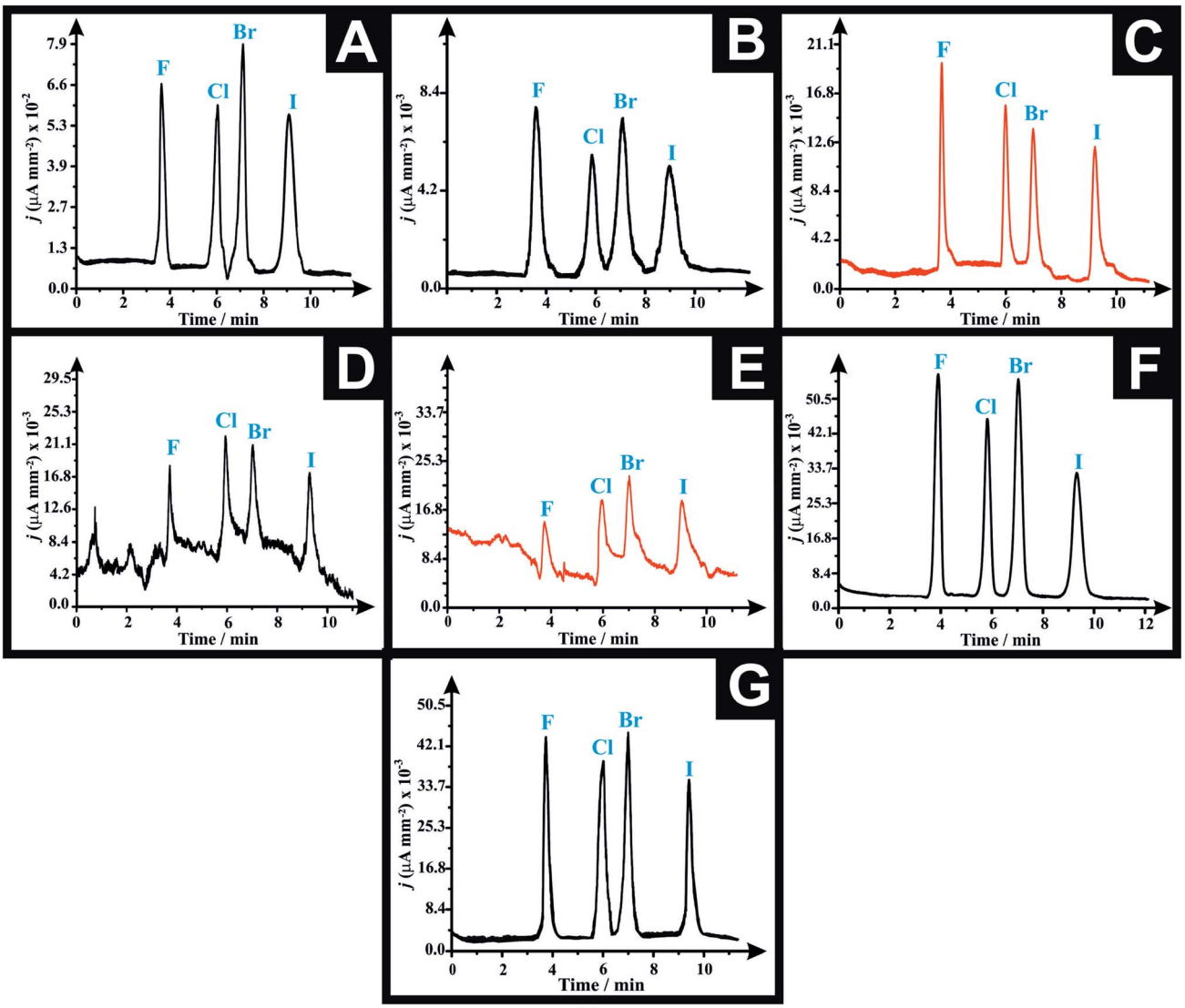

Fig. 3 Representative HPLC-AD amperograms of a solution containing 300 μg mL^{-1} of each of "F": 25F–NBOMe (t_R = 3.84 min), "Cl": 25C–NBOMe (t_R = 5.97 min), "Br": 25B–NBOMe (t_R = 7.02 min) and "I": 25I–NBOMe (t_R = 9.46 min) obtained using ACE C18-AR column (150 × 4.6 mm i.d., particle size: 5 μm), mobile phase: [5 mM ammonium formate + 100 mM KCl (pH 7.0): acetonitrile 70 : 30% v/v], flow rate 2.5 mL min^{-1}, column temperature 60 °C and applied potential: +1.0 V using the proposed AM/3D printed LC-AD wall-jet flow cell utilising the following working electrode substrates (A) graphite screen-printed macroelectrode (SPE); (B) Proto-Pasta (before activation); (C) Proto-Pasta (after activation); (D) Black Magic (before pre-treatment); (E) Black Magic (after pre-treatment); (F) graphite sheet; (G) NG/PLA AM-electrode. Note that the current density j in case of the SPEs in (A) is multiplied by 10^{-2} while it is multiplied by a factor of 10^{-3} in the rest of the tested electrodes.

printed flow cell with our previous findings using the commercial flow cell,[37] treatment of the calibration data of each drug (obtained formerly using the commercial flow cell) was performed in order to obtain plots of current density j (μA mm^{-2}) *vs.* the concentration (μg mL^{-1}) rather than using the current I (μA) (Table 1). In addition, the LODs were calculated based on these generated plots employing the same formula used for all investigated working electrodes (LOD = 3.3Sa/b) (Table 1D). Upon comparing the results, we found that both flow cells have the same linear concentration range for all drugs (20–300 μg mL^{-1}) however, the SPEs sensitivity (slope; b) employing the AM/3D printed flow cell is lower than that obtained utilising the commercial impinging jet flow cell (Table 1B). Additionally, the LODs for the AM/3D printed flow cell were higher than those for the commercial flow cell (Table 1D). The main contributing factor to this was thought to be the flow cell design, especially the larger chamber volume (AM/3D printed flow cell chamber volume: 1200 μL, commercial flow cell chamber volume: 8μL). Where, it was rationalised that the larger sample volume increased sample dispersion, effectively diluting the analytes present at the electrode surface and thereby reducing the sensitivity of the SPE sensor platform *via* transfer/diffusion.[50,51] Concerning the precision of SPEs utilising the newly developed AM/3D flow cell, the repeatability test

revealed satisfactory results as presented by the RSD% which did not exceed 4% (Table S2†).

Proto-Pasta. Commercial graphene-based conductive filament, Proto-Pasta (carbon black/PLA) was tested for the LC-AD of NBOMe derivatives. HPLC-AD amperograms of this printed material exhibited a low background current (Fig. 3B). The sensitivity of this platform was the lowest among all the tested working substrates as presented by the small values of the slopes (Table 1B). Furthermore, the first concentration in the linearity range for all NBOMes was relatively high (50 μg mL^{-1}) (Table 1). Accordingly, to enhance the electrochemical behavior (amperometric response) of this sensor the electrochemical activation described in the literature by Richter *et al.* was followed.[42] This required the application of the potentials +1.4 V for 200 s and −1.0 V for 200 s in 0.5 mol L^{-1} NaOH using two 3D printed Proto-Pasta electrodes as the reference and counter electrodes. Interestingly, a noticeable improvement in the amperometric signal was observed and the peak shapes became sharper and more symmetrical (Fig. 3C). In addition, following the chemical activation, the first concentration in the linear range dropped to 20 μg mL^{-1} and became comparable to SPEs and the slopes for 25F–, 25C–, 25B– and 25I–NBOMe were increased by the following percentages: 127.92%, 156.73%, 72.20% and 134.42%, respectively (Table 1B). Besides, the LOD values for the target analytes were reduced and were better than those obtained by the SPEs in case of both the AM/3D printed and the commercial flow cells (Table 1D). The percentages of decrease in the LODs after the treatment were as follows: 76.38%, 48.28%, 67.29% and 50.82%, for 25F–, 25C–, 25B– and 25I–NBOMe, respectively. The authors attributed the enhancement of the electrochemical response of the pre-treated electrode to changing of the surface characteristics of the Proto-Pasta (carbon black/PLA) electrode.[42] Where, upon carrying out this chemical treatment, the PLA material was partially removed from the electrode surface and the degree of aggregation of carbon black nanoparticles was altered, increasing the nanoparticles exposed to the surface. This was manifested as an increase in the effective electrochemical area of the electrode and hence amplifying the electrochemical response. Regarding the precision of Proto-Pasta electrode, it was observed from the repeatability tests that this working substrate was precise in both conditions (before and after pre-treatment), where the RSD% did not exceed 4% (Table S2†).

Black Magic. The second commercial graphene-based conductive filament evaluated in this study was the so-called, Black Magic (graphene/PLA filament). As can be seen in Fig. 3D, the HPLC-AD amperograms baseline suffered from irregularities and high noise levels. In addition, the calibration curves did not display good linearity as illustrated by the regression coefficient values that ranged from 0.745–0.935 and the first concentration in the linearity range was considerably high (50 μg mL^{-1}) emphasising a poor sensitivity (Table 1C). Also, this electrode demonstrated poor repeatability, as the RSD% were elevated to an extent (RSD% = 4.07–9.65) (Table S2†). Attempts were made in order to enhance the electrochemical performance of the electrode by using the electrochemical pre-treatment procedure reported by dos Santos *et al.*[10] The amperogram shape and the measured amperometric response were not improved (Fig. 3E) and the linearity of the NBOMe calibration curves were noticeably worse, as shown by the regression coefficients (r^2 = 0.467–0.658) (Table 1C). Previously, dos Santos *et al.*[10] were able to improve the electrocatalytic properties of Black Magic electrode towards the detection of dopamine after carrying out the aforementioned pre-treatment step (see Experimental section). This methodology induced structural defects in graphene which led to increasing the exposure of edge planes on the surface. This caused an increase of the density of states (DOS) and improved the electron transfer rates. In addition to this, the pre-treatment steps created oxygen functionalities and elevated the number of sp^2 domains in graphene; which facilitated dopamine interaction *via* hydrogen bond formation and π–π stacking. Evidently, the quantification of NBOMes and the detection limits did not improve after the pre-treatment step. A possible explanation for this could be that these analytes were not surface sensitive to the introduced oxygen functionalities and sp^2 domains and they interacted with the electrode in a different way. Thus, Black Magic AM/3D printed electrode definitely was not the electrode of choice for the reliable quantitation of the target analytes.

Graphite sheets. Silva *et al.*[52] have confirmed that the electrochemical response of industrial graphite sheets can differ significantly and affects the quality of the obtained results. Furthermore, they illustrated that compared to other commercial graphite sheets, the graphite sheets purchased from Panasonic Mouser Electronics (USA) demonstrated superior electrical conductivity, excellent electroanalytical performance, high sensitivity and were used in the as-received conditions without any prior modifications.[52] Moreover, it was proven that this specific kind of graphite sheet can act as an excellent disposable working substrate in electroanalysis and the response of such platform does not change in non-aqueous medium and is comparable to a glassy carbon electrode.[52] Therefore, this type of graphite sheet was tested for the HPLC-AD analysis of NBOMe using our developed AM/3D printed flow cell. It was observed that this working substrate exhibited a low background current, the baseline was very smooth with insignificant noise and the eluted peaks were sharp and symmetrical (Fig. 3F). Concerning the sensitivity, graphite sheet was the second most sensitive sensing platform after the SPEs as demonstrated by the high slope values in Table 1B (with exception to 25F–NBOMe; in which the graphite sheet has the best sensitivity). Moreover, the calculated LOD values were the lowest among all the tested electrodes; even lower than those of the SPEs (in both the AM/3D printed and commercial flow cell) and the pre-treated Proto Pasta (Table 1D). This can be attributed to the high efficiency and excellent performance of this platform which generated calibration plots of good linearity (r^2 = 0.999 for the target analytes) (Table 1C) with smaller errors and deviations in the intercepts (small Sa values) which in turn decreases the LOD values. Owing to the smoothness of the baseline and the low background noise of graphite sheet amperograms, the first concentration in the linearity range that could be quantified practically was lower than that obtained by all platforms tested in this study (10 μg mL^{-1}) (Table 1) and was

Table 1 Comparison of the validation parameters obtained using different electrode substrates employing the proposed AM/3D printed wall-jet flow cell HPLC-AD system for the analytical determination of NBOMe derivatives

	Analyte			
Working electrode	25F–NBOMe	25C–NBOMe	25B–NBOMe	25I–NBOMe
(A) Intercept of the regression line of the calibration curve[a] (μA mm^{-2})				
SPE (AM/3D printed flow cell) linear range: 20–300 μg mL^{-1}	$5.17 \pm 0.81 \times 10^{-3}$	$1.10 \pm 0.82 \times 10^{-3}$	$1.88 \pm 0.55 \times 10^{-3}$	$-8.30 \pm 7.48 \times 10^{-4}$
SPE (commercial flow cell)[37] linear range: 20–300 μg mL^{-1}	$1.93 \pm 0.32 \times 10^{-2}$	$1.18 \pm 0.15 \times 10^{-2}$	$1.13 \pm 0.11 \times 10^{-2}$	$6.13 \pm 0.80 \times 10^{-3}$
Proto-Pasta (before activation) linear range: 50–300 μg mL^{-1}	$6.19 \pm 13.4 \times 10^{-5}$	$3.83 \pm 1.10 \times 10^{-4}$	$2.09 \pm 1.20 \times 10^{-4}$	$1.33 \pm 0.68 \times 10^{-4}$
Proto-Pasta (after activation) linear range: 20–300 μg mL^{-1}	$1.29 \pm 0.07 \times 10^{-3}$	$6.68 \pm 1.46 \times 10^{-4}$	$6.02 \pm 0.67 \times 10^{-4}$	$4.47 \pm 0.78 \times 10^{-4}$
Black Magic (before pre-treatment) linear range: 50–300 μg mL^{-1}	$2.39 \pm 1.38 \times 10^{-3}$	$1.72 \pm 0.97 \times 10^{-3}$	$2.95 \pm 1.38 \times 10^{-3}$	$2.83 \pm 10.60 \times 10^{-4}$
Black Magic (after pre-treatment) linear range: 50–300 μg mL^{-1}	$6.14 \pm 7.13 \times 10^{-3}$	$4.13 \pm 5.06 \times 10^{-3}$	$4.47 \pm 4.14 \times 10^{-3}$	$2.84 \pm 3.21 \times 10^{-3}$
Graphite sheet linear range: 10–300 μg mL^{-1}	$2.51 \pm 0.18 \times 10^{-3}$	$4.48 \pm 2.12 \times 10^{-4}$	$1.09 \pm 0.21 \times 10^{-3}$	$2.12 \pm 1.35 \times 10^{-4}$
NG/PLA AM-electrode linear range: 20–300 μg mL^{-1}	$-5.33 \pm 6.79 \times 10^{-4}$	$-1.21 \pm 5.97 \times 10^{-4}$	$-1.59 \pm 0.56 \times 10^{-3}$	$-9.38 \pm 4.31 \times 10^{-4}$
(B) The slope of the regression line of the calibration curve[b] (μA mL mm^{-2} μg^{-1})				
SPE (AM/3D printed flow cell) linear range: 20–300 μg mL^{-1}	$1.83 \pm 0.05 \times 10^{-4}$	$1.76 \pm 0.05 \times 10^{-4}$	$1.79 \pm 0.03 \times 10^{-4}$	$1.67 \pm 0.05 \times 10^{-4}$
SPE (commercial flow cell)[37] linear range: 20–300 μg mL^{-1}	$7.49 \pm 0.20 \times 10^{-4}$	$3.78 \pm 0.09 \times 10^{-4}$	$4.88 \pm 0.07 \times 10^{-4}$	$3.16 \pm 0.05 \times 10^{-4}$
Proto-Pasta (before activation) linear range: 50–300 μg mL^{-1}	$2.40 \pm 0.07 \times 10^{-5}$	$1.71 \pm 0.06 \times 10^{-5}$	$2.23 \pm 0.07 \times 10^{-5}$	$1.54 \pm 0.04 \times 10^{-5}$
Proto-Pasta (after activation) linear range: 20–300 μg mL^{-1}	$5.47 \pm 0.04 \times 10^{-5}$	$4.39 \pm 0.09 \times 10^{-5}$	$3.84 \pm 0.04 \times 10^{-5}$	$3.61 \pm 0.05 \times 10^{-5}$
Black Magic (before pre-treatment) linear range: 50–300 μg mL^{-1}	$3.53 \pm 0.76 \times 10^{-5}$	$3.13 \pm 0.53 \times 10^{-5}$	$2.24 \pm 0.76 \times 10^{-5}$	$3.82 \pm 0.58 \times 10^{-5}$
Black Magic (after pre-treatment) linear range: 50–300 μg mL^{-1}	$6.82 \pm 3.92 \times 10^{-5}$	$4.52 \pm 2.78 \times 10^{-5}$	$3.84 \pm 2.28 \times 10^{-5}$	$4.25 \pm 1.77 \times 10^{-5}$
Graphite sheet linear range: 10–300 μg mL^{-1}	$1.89 \pm 0.01 \times 10^{-4}$	$1.59 \pm 0.01 \times 10^{-4}$	$1.38 \pm 0.01 \times 10^{-4}$	$1.11 \pm 0.01 \times 10^{-4}$
NG/PLA AM-electrode linear range: 20–300 μg mL^{-1}	$1.48 \pm 0.04 \times 10^{-4}$	$1.22 \pm 0.04 \times 10^{-4}$	$1.29 \pm 0.03 \times 10^{-4}$	$9.85 \pm 0.26 \times 10^{-5}$
(C) Coefficient of regression (r^2)				
SPE (AM/3D printed flow cell) linear range: 20–300 μg mL^{-1}	0.997	0.997	0.999	0.997
SPE (commercial flow cell)[37] linear range: 20–300 μg mL^{-1}	0.997	0.997	0.999	0.999

Table 1 (*Contd.*)

	Analyte			
Working electrode	25F–NBOMe	25C–NBOMe	25B–NBOMe	25I–NBOMe
Proto-Pasta (before activation) linear range: 50–300 μg mL^{-1}	0.997	0.996	0.997	0.998
Proto-Pasta (after activation) linear range: 20–300 μg mL^{-1}	0.999	0.998	0.999	0.999
Black Magic (before pre-treatment) linear range: 50–300 μg mL^{-1}	0.878	0.920	0.745	0.935
Black Magic (after pre-treatment) linear range: 50–300 μg mL^{-1}	0.501	0.467	0.486	0.658
Graphite sheet linear range: 10–300 μg mL^{-1}	0.999	0.999	0.999	0.999
NG/PLA AM-electrode linear range: 20–300 μg mL^{-1}	0.997	0.997	0.997	0.997
(D) Limit of detection (LOD)[d] (μg mL^{-1})				
SPE (AM/3D printed flow cell) linear range: 20–300 μg mL^{-1}	14.67 ± 0.40	15.32 ± 0.44	10.20 ± 0.17	14.79 ± 0.44
SPE (commercial flow cell)[37] linear range: 20–300 μg mL^{-1}	14.22 ± 0.40	13.07 ± 0.31	7.63 ± 0.11	8.34 ± 0.13
Proto-Pasta (before activation) linear range: 50–300 μg mL^{-1}	18.42 ± 0.54	21.19 ± 0.74	17.73 ± 0.56	14.58 ± 0.38
Proto-Pasta (after activation) linear range: 20–300 μg mL^{-1}	4.35 ± 0.03	10.96 ± 0.22	5.80 ± 0.06	7.17 ± 0.10
Black Magic (before pre-treatment) linear range: 50–300 μg mL^{-1}	n.d.[c]	n.d.[c]	n.d.[c]	n.d.[c]
Black Magic (after pre-treatment) linear range: 50–300 μg mL^{-1}	n.d.[c]	n.d.[c]	n.d.[c]	n.d.[c]
Graphite sheet linear range: 10–300 μg mL^{-1}	3.16 ± 0.02	4.39 ± 0.03	5.02 ± 0.04	4.01 ± 0.04
NG/PLA AM-electrode linear range: 20–300 μg mL^{-1}	15.16 ± 0.41	16.11 ± 0.53	14.43 ± 0.34	14.44 ± 0.38

[a] Intercept ± standard error. [b] Slope ± standard error. [c] n.d.: not detected. [d] LOD = (3.3 × Sa)/*b*; where Sa: standard deviation of intercept, *b*: slope of the regression line of the calibration curve.

Table 2 Comparison between the quantitative data obtained by different electrode substrates employing the proposed AM/3D printed wall-jet flow cell HPLC-AD system for the analytical determination of NBOMes in simulated blotter papers

			Drug recovered			
Sample	Working electrode	Parameter	LSD	25F–NBOMe	25B–NBOMe	25I–NBOMe
(A) Blotter paper I						
		t_R (min.) ± SD[a]	2.78 ± 0.03	3.84 ± 0.05	7.02 ± 0.04	9.46 ± 0.06
Blotter paper I	SPEs	Mean % R ± SD[b]	+	−	−	100.1 ± 2.65
		RSD%[c]	+	−	−	2.65
		E_r (%)[d]	+	−	−	0.1
	Activated Proto-Pasta	Mean % R ± SD[b]	+	−	−	96.11 ± 3.34
		RSD%[c]	+	−	−	3.48
		E_r (%)[d]	+	−	−	−3.89
	Graphite sheet	Mean % R ± SD[b]	+	−	−	99.84 ± 1.42
		RSD%[c]	+	−	−	1.42
		E_r (%)[d]	+	−	−	−0.16
	NG/PLA AM-electrode	Mean % R ± SD[b]	+	−	−	96.90 ± 0.13
		RSD%[c]	+	−	−	0.13
		E_r (%)[d]	+	−	−	−3.1
(B) Blotter paper II						
		t_R (min.) ± SD[a]	2.78 ± 0.05	3.84 ± 0.02	7.02 ± 0.09	9.46 ± 0.08
Blotter paper II	SPEs	Mean % R ± SD[b]	+	99.83 ± 2.12	−	103.0 ± 1.92
		RSD%[c]	+	2.12	−	1.86
		E_r (%)[d]	+	−0.17	−	3.00
	Activated Proto-Pasta	Mean % R ± SD[b]	+	98.35 ± 1.51	−	98.74 ± 1.39
		RSD%[c]	+	1.54	−	1.41
		E_r (%)[d]	+	−1.65	−	−1.26
	Graphite sheet	Mean % R ± SD[b]	+	100.3 ± 0.89	−	99.05 ± 1.71
		RSD%[c]	+	0.89	−	1.73
		E_r (%)[d]	+	0.27	−	−0.95
	NG/PLA AM-electrode	Mean % R ± SD[b]	+	102.8 ± 2.39	−	98.93 ± 0.53
		RSD%[c]	+	2.33	−	0.54
		E_r (%)[d]	+	2.76	−	−1.07
(C) Blotter paper III						
		t_R (min.) ± SD[a]	2.78 ± 0.07	3.84 ± 0.04	7.02 ± 0.08	9.46 ± 0.08
Blotter paper III	SPEs	Mean % R ± SD[b]	−	−	98.47 ± 1.02	−
		RSD%[c]	−	−	1.04	−
		E_r (%)[d]	−	−	−1.53	−
	Activated Proto-Pasta	Mean % R ± SD[b]	−	−	100.3 ± 3.33	−
		RSD%[c]	−	−	3.32	−
		E_r (%)[d]	−	−	0.26	−
	Graphite sheet	Mean % R ± SD[b]	−	−	101.1 ± 1.43	−
		RSD%[c]	−	−	1.42	−
		E_r (%)[d]	−	−	1.05	−
	NG/PLA AM-electrode	Mean % R ± SD[b]	−	−	100.4 ± 0.58	−
		RSD%[c]	−	−	0.58	−
		E_r (%)[d]	−	−	0.37	−

[a] t_R (min.) ± SD: retention time (minutes) for each eluted drug in the amperogram ± standard deviation (SD) of three determinations. [b] Mean % recovery ± SD of three determinations for each drug detected in each blotter paper. [c] % relative standard deviation of three determinations for each drug detected in each blotter paper. [d] % relative error; (+) = present in the blotter paper sample; (−) absent from the blotter paper sample.

equivalent to that obtained by HPLC-DAD reported in our previous work,[37] emphasizing the high sensitivity and reliability of graphite sheets in analytical quantification. The graphite sheets demonstrated excellent repeatability, which was apparent in the values of RSD% that did not exceed 2% (Table S2†). Thus, graphite sheets represented a reliable, sensitive, robust and cost-effective disposable sensing platform that could be easily integrated with the designed AM/3D printed flow cell for forensic and routine analytical measurements.

NG/PLA AM-electrode. This bespoke 3D printed sensing platform was formerly examined in our previous work for the simultaneous quantification of lead and cadmium.[40] It was illustrated that this sensor had extremely low quantities of the loaded electrochemically active material (25% w/w nanographite-NG) but still demonstrated useful electrochemical behaviour and sufficient conductivity. An NG percentage between 20–25 wt. was optimum for better percolation, greater conductivity, seamless printability and thus

providing more reproducible AM/3D prints.[40] Noticeably, increasing the NG% beyond this limit resulted in a brittle filament and uneven printing process which was unsuitable to be exploited in this study due to leakages that would occur.[40] Upon testing the AM/3D printed electrode for the HPLC-AD of NBOMe, it was found that the amperogram possessed a good baseline and the background current was low indicating good electrochemical properties of the electrode material (Fig. 3G). The electrode exhibited good sensitivity as the slopes of the NBOMes calibration curves were satisfactory, better than those of the pre-treated Proto Pasta, but still lower than those of the SPEs and the graphite sheet (Table 1B). The first concentration that could be quantified practically was equivalent to 20 μg mL^{-1} (Table 1), the same as the SPEs and the pre-treated Proto Pasta. Moreover, the repeatability test performed exhibited good results, where the RSD% did not exceed 4% (Table S2†).

Forensic application

Application to simulated blotter papers. NBOMe simulated blotter papers were used to evaluate the analytical performance of the developed AM/3D printed LC-AD wall-jet flow cell system. The four working substrates that demonstrated superior electroanalytical behaviour, namely, SPEs, pre-treated Proto-Pasta, graphite sheet and NG/PLA AM-electrode were investigated. According to the literature, most recreated NBOMe blotters contained doses of 500–800 μg per blotter (ref. 53) and the size of the seized blotters were usually in the range of (0.5×0.5 cm^2 to 1×1 cm^2).[54] Accordingly, we prepared 3 different simulated blotter papers (each blotter was prepared in triplicate) using concentrations of 500 and 600 μg per blotter of NBOMes. Lysergic acid diethylamide (LSD) was added to 2 blotters in order to simulate real samples. The drugs were extracted from the blotters with methanol and then the samples were half diluted with the mobile phase to obtain concentrations within the linearity ranges and then analysis was carried out. As can be seen in Table 2A–C, each drug eluted at its designated retention time (t_R) when utilising the AM/3D printed flow cell. The four tested electrodes exhibited good analytical performance and high accuracy, as illustrated by the values of recovery% (R%) and error% (E_r%) that ranged from; %R = 98.47–103% (E_r% = −1.53 − (+3.0)) for SPEs, 96.11–100.26% (E_r% = −3.89 − (+0.26)) for activated Proto-Pasta, 99.05–101.05% (E_r% = −0.95 − (+1.05)) for graphite sheets and 96.90–102.76% (E_r% = −3.0 − (+2.76)) for NG/PLA AM-electrode. Moreover, good precision of the AM/3D printed flow cell and the examined electrodes was demonstrated by the low RSD% values, which were in the following ranges: 1.04–2.65% for SPEs, 1.41–3.48% for activated Proto-Pasta, 0.89–1.73% for graphite sheet and 0.13–2.33% for NG/PLA AM-electrode (Table 2A–C).

By careful investigation of the obtained results it was deduced that these four working substrates can work efficiently in combination with the proposed AM/3D printed flow cell for the electroanalytical quantification of a wide range of compounds in quality control labs. The best analytical performance was attributed to the SPEs and the graphite sheet. This is attributed to the increased electrochemically active sites presented by these two working electrode platforms, in addition to their high sensitivity, reproducibility, ease-of-use and scalability of production,[55] noting that the former are mainly comprised of plastic with lesser electrochemically active sites.

Conclusions

Herein, we have reported for the first time the fabrication of a versatile wall-jet AM/3D printed flow cell that was designed especially for liquid chromatography-amperometric detection (LC-AD). The flow cell was optimised in terms of the design, geometry and the distance between the HPLC outlet PTFE tubing and the electrode surface. Additionally, the flow cell was evaluated by analyzing a mixture of four NBOMe derivatives utilising five working substrates; namely, SPEs, Proto-Pasta (before and after chemical activation), Black Magic (before and after chemical pre-treatment), graphite sheets and NG/PLA AM-electrode. The analytical performance of the AM/3D printed flow cell was compared with our previous report using a commercial impinging jet-flow cell incorporating SPEs as the working electrode material. Interestingly, the AM/3D printed flow cell had several advantages over the commercial systems. These included the simple geometrical configuration, short production time, low cost, higher sensitivity of the wall-jet design, efficient mass transport of the analyte onto the electrode surface, simple assembly, versatility toward working electrode substrates and high flow rate tolerance (2.5 mL min^{-1}). This platform also provides flexibility in 3D designing, which permits simple modification of the flow cell configuration for the application to more specific electrode geometries and sizes.

Regarding the working substrates tested in this study, it was demonstrated that the SPEs were the best working platform. They are not as sensitive as when using them incorporated into the commercial flow cell, however they still demonstrate a beneficial electrochemical response. The second best working platform was the graphite sheet; its sensitivity was comparable to the HPLC-DAD results published in our previous work, in addition to the sharp and symmetrical peaks of the obtained amperogram. The homemade conductive NG/PLA AM-electrode was the third-best sensor in term of sensitivity followed by the pre-treated Proto-Pasta electrode. The worst was the Black Magic working substrate that did not display a better amperometric response even after chemical pre-treatment. To sum up, the proposed AM/3D printed wall-jet flow cell accompanied with the SPEs, graphite sheet, NG/PLA AM-electrode and pre-treated Proto-Pasta working substrates can make a promising reliable and sensitive analytical tool that could be integrated within liquid chromatographic systems for the cost-effective electrochemical detection and quantification of various analytes in quality control and forensic laboratories.

Conflicts of interest

There are no conflicts to declare.

Acknowledgements

We sincerely thank Newton-Mosharafa PhD Scholarship, funded by both the Egyptian Ministry of Higher Education and the British Council for supporting this research. Funding from the Engineering and Physical Science Research Council (Reference: EP/N001877/1) and a British Council Institutional Grant Link (No. 172726574) is acknowledged. Also, the authors would like to thank Dr Oliver B. Sutcliffe, Faculty of Science and Engineering, Manchester Metropolitan University, for providing the standard NBOMe drug samples to accomplish this work.

References

1 T. D. Ngo, A. Kashani, G. Imbalzano, K. T. Q. Nguyen and D. Hui, *Composites, Part B*, 2018, **143**, 172–196.
2 R. M. Cardoso, D. M. H. Mendonça, W. P. Silva, M. N. T. Silva, E. Nossol, R. A. B. da Silva, E. M. Richter and R. A. A. Muñoz, *Anal. Chim. Acta*, 2018, **1033**, 49–57.
3 A. Ambrosi and M. Pumera, *Chem. Soc. Rev.*, 2016, **45**, 2740–2755.
4 A. A. Sheikh, *Virtual Phys. Prototyping*, 2015, **10**, 175–185.
5 S. V. Murphy and A. Atala, *Nat. Biotechnol.*, 2014, **32**, 773.
6 C. Parra-Cabrera, C. Achille, S. Kuhn and R. Ameloot, *Chem. Soc. Rev.*, 2018, **47**, 209–230.
7 C.-K. Su, P.-J. Peng and Y.-C. Sun, *Anal. Chem.*, 2015, **87**, 6945–6950.
8 B. Gross, S. Y. Lockwood and D. M. Spence, *Anal. Chem.*, 2017, **89**, 57–70.
9 C. L. Manzanares Palenzuela and M. Pumera, *TrAC, Trends Anal. Chem.*, 2018, **103**, 110–118.
10 P. L. dos Santos, V. Katic, H. C. Loureiro, M. F. dos Santos, D. P. dos Santos, A. L. B. Formiga and J. A. Bonacin, *Sens. Actuators, B*, 2019, **281**, 837–848.
11 D. M. H. Mendonça, D. P. Rocha, G. S. V. Dutra, R. M. Cardoso, A. D. Batista, E. M. Richter and R. A. A. Munoz, *Electroanalysis*, 2019, 31, 771-777.
12 S. A. Gowers, V. F. Curto, C. A. Seneci, C. Wang, S. Anastasova, P. Vadgama, G. Z. Yang and M. G. Boutelle, *Anal. Chem.*, 2015, **87**, 7763–7770.
13 P. R. Miller, S. A. Skoog, T. L. Edwards, D. M. Lopez, D. R. Wheeler, D. C. Arango, X. Xiao, S. M. Brozik, J. Wang, R. Polsky and R. J. Narayan, *Talanta*, 2012, **88**, 739–742.
14 M. Areir, Y. Xu, D. Harrison and J. Fyson, *Mater. Sci. Eng., B*, 2017, **226**, 29–38.
15 M. D. Symes, P. J. Kitson, J. Yan, C. J. Richmond, G. J. T. Cooper, R. W. Bowman, T. Vilbrandt and L. Cronin, *Nat. Chem.*, 2012, **4**, 349–354.
16 https://www.metrohm.com/en-gb/products-overview/electrochemistry/cells-for-electrochemistry/, accessed August 2019.
17 https://antecscientific.com/uhplc-with-electrochemical-detection-lc-ecd/flow-cells, accessed August 2019.
18 https://www.basinc.com/products/ec/flowcells, accessed August 2019.
19 http://www.erc-hplc.de/en/lc-detectors/ec-detector-ec-flowcells/electrochemical-flow-cells.html, accessed August 2019.
20 J. S. Stefano, R. H. O. Montes, E. M. Richter and R. A. A. Muñoz, *J. Braz. Chem. Soc.*, 2014, **25**, 484–491.
21 Y. Murakami, T. Takeuchi, K. Yokoyama, E. Tamiya, I. Karube and M. Suda, *Anal. Chem.*, 1993, **65**, 2731–2735.
22 Z. Jinjin, C. Ming, Y. Caixia and T. Yifeng, *Analyst*, 2011, **136**, 4070–4074.
23 H. Deng and G. J. V. Berkel, *Electroanalysis*, 1999, **11**, 857–865.
24 Y. X. Chen, M. Heinen, Z. Jusys and R. J. Behm, *Angew. Chem., Int. Ed.*, 2006, **45**, 981–985.
25 L. Gomes, D. W. Miwa, G. R. P. Malpass and A. J. Motheo, *J. Braz. Chem. Soc.*, 2011, **22**, 1299–1306.
26 T. Noyhouzer and D. Mandler, *Electroanalysis*, 2013, **25**, 109–115.
27 P. L. Joynes and R. J. Maggs, *J. Chromatogr. Sci.*, 1970, **8**, 427–433.
28 A. T. Hubbard and F. C. Anson, *Electroanalytical Chemistry*, ed. A. J. Bard, 1970, vol. 4, pp. 129–214.
29 J. Yamada and H. Matsuda, *J. Electroanal. Chem. Interfacial Electrochem.*, 1973, **44**, 189–198.
30 K. Brunt, C. H. P. Bruins, D. A. Doornbos and B. Oosterhuis, *Anal. Chim. Acta*, 1980, **114**, 257–266.
31 B. Oosterhuis, K. Brunt, B. H. C. Westerink and D. A. Doornbos, *Anal. Chem.*, 1980, **52**, 203–205.
32 K. B. Spilstead, J. J. Learey, E. H. Doeven, G. J. Barbante, S. Mohr, N. W. Barnett, J. M. Terry, R. M. Hall and P. S. Francis, *Talanta*, 2014, **126**, 110–115.
33 I. Lozano, C. López, N. Menendez, N. Casillas and P. Herrasti, *J. Electrochem. Soc.*, 2018, **165**, h688–h697.
34 P. Nikolaou, I. Papoutsis, M. Stefanidou, C. Spiliopoulou and S. Athanaselis, *Drug Chem. Toxicol.*, 2015, **38**, 113–119.
35 K. G. Shanks, T. Sozio and G. S. Behonick, *J. Anal. Toxicol.*, 2015, **39**, 602–606.
36 A. Al-Imam, *Iran. J. Psychiatry Behav. Sci.*, 2018, **12**, e9870.
37 H. M. Elbardisy, C. W. Foster, J. Marron, R. E. Mewis, O. B. Sutcliffe, T. S. Belal, W. Talaat, H. G. Daabees and C. E. Banks, *ACS Omega*, 2019, **4**, 14439–14450.
38 Tinkercad|Create 3D digital designs with online CAD, 2019, https://www.tinkercad.com/, accessed February 2019.
39 F. E. Galdino, C. W. Foster, J. A. Bonacin and C. E. Banks, *Anal. Methods*, 2015, **7**, 1208–1214.
40 C. W. Foster, H. M. Elbardisy, M. P. Down, E. M. Keefe, G. C. Smith and C. E. Banks, *Chem. Eng. J.*, 2019, 122343, DOI: 10.1016/j.cej.2019.122343.
41 K. Y. Zuway, J. P. Smith, C. W. Foster, N. Kapur, C. E. Banks and O. B. Sutcliffe, *Analyst*, 2015, **140**, 6283–6294.
42 E. M. Richter, D. P. Rocha, R. M. Cardoso, E. M. Keefe, C. W. Foster, R. A. A. Munoz and C. E. Banks, *Anal. Chem.*, 2019, **91**, 12844–12851.
43 A. F. B. Andrade, S. K. Mamo and J. Gonzalez-Rodriguez, *Anal. Chem.*, 2017, **89**, 1445–1452.
44 M. Trojanowicz, *Anal. Chim. Acta*, 2011, **688**, 8–35.
45 R. G. Compton, A. C. Fisher, M. H. Latham, C. M. A. Brett and A. M. C. F. O. Brett, *J. Phys. Chem.*, 1992, **96**, 8363–8367.
46 J. C. Ball, R. G. Compton and C. M. A. Brett, *J. Phys. Chem. B*, 1998, **102**, 162–166.
47 K. Honeychurch, *Separations*, 2016, **3**, 28.

48 Z. Niegreisz, L. Szücs, J. Fekete, G. Horvai, K. Tóth and E. Pungor, *J. Chromatogr. A*, 1984, **316**, 451–459.
49 H. Gunasingham and B. Fleet, *Anal. Chem.*, 1983, **55**, 1409–1414.
50 R. Guidelli, *J. Electroanal. Chem. Interfacial Electrochem.*, 1971, **33**, 291–302.
51 R. Guidelli, *J. Electroanal. Chem. Interfacial Electrochem.*, 1971, **33**, 303–317.
52 L. A. J. Silva, J. S. Stefano, R. M. Cardoso, N. S. Prado, P. H. T. Soares, E. Nossol, R. A. A. Munoz, L. Angnes and E. M. Richter, *J. Electroanal. Chem.*, 2019, **833**, 560–567.
53 J. L. Poklis, S. A. Raso, K. N. Alford, A. Poklis and M. R. Peace, *J. Anal. Toxicol.*, 2015, **39**, 617–623.
54 G. A. Souza, L. C. Arantes, T. J. Guedes, A. C. de Oliveira, P. A. Marinho, R. A. A. Muñoz and W. T. P. dos Santos, *Electrochem. Commun.*, 2017, **82**, 121–124.
55 A. García-Miranda Ferrari, C. W. Foster, P. J. Kelly, D. A. Brownson and C. E. Banks, *Biosensors*, 2018, **8**, 53.